INSTITUTE OF PHYSICS PUBLISHING NANOTECHNOLOGY
Nanotechnology **15** (2004) S55–S59 PII: S0957-4484(04)68559-X

Reversible short-range electrostatic imaging in frequency modulation atomic force microscopy on metallic surfaces

Peter Dieška[1], Ivan Štich[1] and Rubén Pérez[2]

[1] Centre for Computational Materials Science (CCMS), Slovak University of Technology (FEI STU), Ilkovičova 3, SK-812 19, Bratislava, Slovakia
[2] Departamento de Física Teórica de la Materia Condensada, Universidad Autónoma de Madrid, E-28049 Madrid, Spain

Received 28 August 2003, in final form 20 November 2003
Published 13 January 2004
Online at stacks.iop.org/Nano/15/S55 (DOI: 10.1088/0957-4484/15/2/012)

Abstract
The mechanism of atomic-scale image formation in non-contact AFM on metallic surfaces is analysed using total-energy pseudopotential calculations. Depending on the tip–apex configuration, we find two different imaging modes. Both clean and metal contaminated Si tips provide atomic resolution arising from the very strong covalent tip–sample interaction, in striking similarity with the imaging mechanism found on semiconductor surfaces. A completely new mechanism, reversible short-range electrostatic imaging, due to subtle charge-transfer interactions is identified for oxidized Si tips. Contrary to the strong covalent-bond imaging, this new mechanism causes only negligible surface perturbation and can account for recent experimental results.

1. Introduction

In the last few years, frequency modulation (FM) atomic force microscopy (AFM) [1, 2] (also called non-contact (NC) AFM) has developed to become a powerful technique for obtaining atomic-scale images of semiconductor (e.g. Si(111) [2], Si(001) [3], polar InP [4, 5], GaAs [6], InAs [7]) and insulating surfaces (e.g. alkali halides [8, 9]) in UHV. In the FM–AFM technique [10, 11], an electronic gain control circuit keeps the cantilever oscillating always with a constant amplitude at its current resonance frequency, and the surface-related information is inferred precisely from the frequency shift (the variation with respect to the cantilever natural resonance frequency for free oscillation) due to the tip–surface interaction.

The key question in FM–AFM, as in any other scanning probe microscope technique, is the relation between the atomic-scale features observed in the topographical images and the source of contrast, the tip–surface interaction in the case of AFM or the tunnelling current in the case of scanning tunnelling microscopy (STM). Theoretical modelling is thus needed in order to understand the mechanism of atomic-scale resolution, interpret the experimental images, and to extend the application of the FM–AFM to a wider range of systems.

Theory has provided a very strong indication that on reactive semiconductor surfaces the short-range chemical tip–surface interaction significantly enhances the atomic resolution of the FM–AFM [12–16]. This interaction can be thought of as dangling bond–dangling bond type of interaction [13]. Experiments have shown that the observed image reflects the variation of local reactivity between the tip and the sample [17–21] and thus have corroborated the theoretical predictions. A detailed quantitative comparison between theory and low temperature FM–AFM measurements on the adatoms of the Si(111)-7 $\times$ 7 reconstruction [10, 19, 20] confirms that the measured short-range interaction is precisely that of a single tip dangling bond interacting with the adatom dangling bond.

On the other hand, on ionic surfaces, such as NaCl, MgO or LiF, the atomic resolution has been shown to arise primarily from short-range electrostatic interactions [22]. A combined experimental and theoretical work on the $CaF_2(111)$ surface [23, 24] has recently established an unambiguous identification of the sublattices imaged by force microscopy in an insulator.

In spite of the fact that FM–AFM can, at least in principle, be used for atomic-scale imaging of insulating, semiconducting, and metallic surfaces alike, the first applications of the technique to metal surfaces have appeared

relatively recently. True atomic-scale images of copper surfaces have been presented by Loppacher *et al* [25, 26] and of Ag(111) by Orisaka *et al* [27]. Imaging metals with any scanning probe (even STM) is challenging because of the short interatomic distances and low charge corrugation. It is then a test on the resolution capabilities of the FM–AFM. Furthermore, as the tunnelling current can be simultaneously collected during the FM–AFM operation on metallic surfaces, the information and performance provided by the two techniques (FM–AFM and STM) can be compared.

On metallic surfaces, the contrast mechanisms are expected to be different from those discussed above for semiconductors and insulators. The delocalized nature of valence electronic charge on metals surfaces is less likely to lead to the spatially very localized tip–surface interaction which was behind the atomic resolution on semiconductor surfaces, and for the same reason is unlikely to lead to spatial variation of electrostatic potential across the surface as was the case on alkali halide surfaces. These arguments seem to suggest that a completely different mechanism and model needs to be evoked for understanding FM–AFM results for each of the three groups of surfaces. To the best of our knowledge, unlike the case for semiconductors and insulators where studies and models are already readily available, no realistic atomistic study of the FM–AFM imagining mechanism exists for metallic surfaces.

One might hope to benefit from the experience acquired in understanding the STM images of related metals surfaces. Unfortunately, even here the situation is not fully understood. In order to explain the first STM images of (111) surfaces of Au and Al [28, 29], special tip-induced effects had to be invoked [30]. The recent combined dynamic FM–AFM/STM experiments [26] on Cu surfaces contributed further puzzles. They yield images with atomic resolution but with estimated chemical forces about an order of magnitude smaller than expected and decay lengths factors for tunnelling currents (λ_T) and tip–surface forces (λ_F) about a factor of three larger than expected and $\lambda_F = 2\lambda_T$. These experimental findings call for a clear understanding of the mechanism behind the observed atomic resolution imaging on metallic surfaces.

To this point we use a case study, Cu(001) surface [25, 26], to conduct a search for the imaging mechanism. Our main finding is that the existing experimental results [25, 26] can only be accounted for by assuming the presence of a weak type of tip–surface forces, arising from *reversible short-range charge-transfer processes* between an oxidized Si tip and the metal surface. This mechanism provides atomic resolution with negligible surface perturbation. In contrast, clean Si tips provide a very strong, spatially localized covalent bond that can easily lead to tip contamination. Both clean and metal contaminated tips provide a covalent tip–sample interaction that results in an imaging mechanism very similar to that found on semiconducting surfaces. Some aspects of the present work were presented in [31].

The rest of the paper is organized as follows. In section 2 we discuss the modelling of the different tips and the metallic surface and the details of our first-principles calculations of the tip–sample interaction. Section 3 presents the results for the total energy and forces on approach curves at different symmetry points on the metal surface for the different tips considered. We conclude in section 4 with a discussion of these results in light of the experiments and of the application of the newly found imaging mechanism to other surfaces.

2. Tip–sample interaction modelling and computational details

Our model for the tip–surface interaction is based on the division [12, 13, 22] of the tip into a macroscopic part which contributes mainly the long-range background interaction, such as van der Waals, and a nano-tip which is responsible for short-range forces. The background long-range interactions depend on the details of the tip, which can be taken from experiments [32].

As Si tips have been used in the experiments [25, 26], we model the nano-termination of the tip by a small (4-atom) Si nano-asperity saturated at the base by H atoms [12, 13] (see the inset in figure 1(a)). The main characteristic of such a Si nano-tip is the presence of one singly occupied dangling bond sticking out of the tip–apex. The dangling bond was found instrumental for atomic resolution of FM–AFM on reactive surfaces [12, 13]. We have also considered other tip terminations which may result from contamination by impurities from the vacuum chamber or surface material. Two examples are shown in figures 1(b), (c). The first tip has a Cu atom built in into the Si tip as an apex. Such an apex may form from tip crash into the surface. The other tip has an apex formed by a Cu atom removed from the surface and bonded to the Si apex. Our simulations (see section 3) show that such an apex will readily form on Cu surfaces.

Si tips in ambient conditions are covered by a thin oxide layer. This situation represents a very complex tip termination. Several models for the SiO_2 surface exist [33]. They all share the following features: (a) twofold O and fourfold Si coordination, and (b) O protruding out of the SiO_2 layer. Therefore, in order to explore the imaging of a metallic surface with an oxidized tip we have considered the simplest, yet realistic model, to describe the tip termination, namely an H_2O molecule. The oxygen atom points towards the scanned surface, as would be the case in an oxidized tip. The H-termination mimics the local twofold coordination and chemistry of the O apex in the oxide layer. In particular, as in the SiO_2 layer, the oxygen will be left with two lone-pair electrons. Such a tip construction, focusing on the key ingredients, closely follows the philosophy behind the other commonly used model tips, such as the Si tip [12, 13, 24] or the MgO tip [22].

As regards the sample, we use a four (double)layers thick slab model with a 3×3 surface unit cell to describe the surface. In the z-direction the periodic images were separated by a vacuum region. The calculation of the tip–surface force versus distance curves is performed by stepwise displacements of the model tip towards the surface. At each tip position the structure of the interacting tip–surface system is relaxed, and the tip–surface force calculated. In the structural relaxation the atoms in the bottom surface layer are kept fixed to emulate the proper surface termination. In all model tips only the apex atom and apex bonded impurity, where present, were allowed to relax. The normal force acting on the tip is calculated as a numerical derivative of the energy curve. We

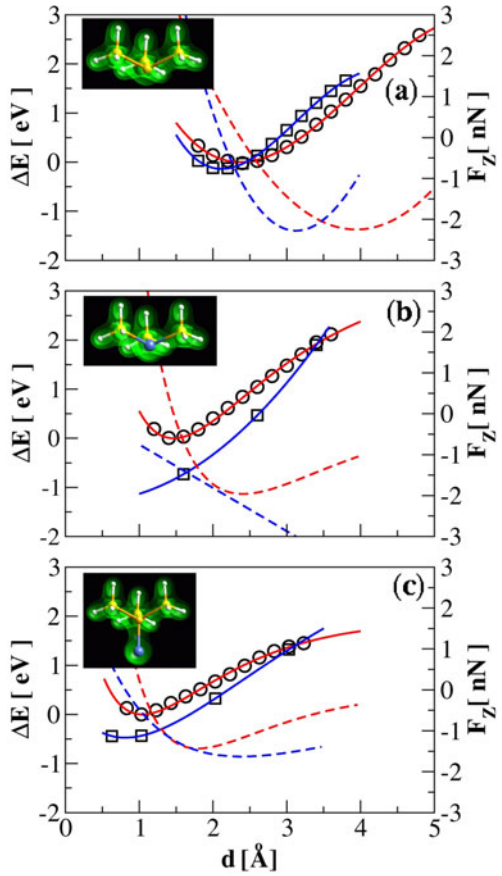

Figure 1. Scans of short-range tip–surface energy over on-top (red colour, circles) and hollow sites (blue colour, boxes) and normal force (red and blue broken curves). The full curves are fits to the computed data. (a) Scans with pure Si tip, (b) Si tip terminated by Cu apex, and (c) Si tip terminated by Cu impurity removed from the surface. d corresponds to tip–surface distance [13]. The minimum of the energy curves over on-top sites is taken as zero. The insets show the tips with two typical isosurfaces of constant (valence) electronic charge density.

consider no applied voltage [34]. The energies and forces were calculated within the density functional theory (DFT) in its plane-wave pseudopotential formulation [35] using the CASTEP suite of codes[3]. All atoms were described by ultrasoft pseudopotentials [36]. We use a gradient corrected functional for the exchange–correlation energy [38]. The wavefunctions were expanded on a mesh of two Monkhorst–Pack k-points [39] with a plane-wave cut-off of 270 eV. A smearing width of $\sigma = 0.2$ eV was used [40]. Standard tests show that this set of parameters provides a very accurate description of the system. We have found that a dipole is formed when the tip approaches the surface. However, the change of the dipole as a function of the tip–surface distance is negligible. Hence, the results are not affected by spurious dipole image interactions [41].

3. Results

Our results for vertical scans over on-top and hollow sites of the Cu(001) surface with a pure Si tip are shown in figure 1(a). The magnitude and range of the tip–surface forces (≈2 nN, 3 Å) and interaction energies (≈2 eV) are characteristic of a strong *covalent bond*. This striking result is further depicted in figure 2, showing the interaction of the Si tip with the Cu(001). This interaction is almost indistinguishable from that found for a reactive semiconductor surface [12, 15, 16]. Hence, despite the more delocalized reactive charge, a very well localized covalent bond between the tip and the metal surface is formed. This covalent bond is formed by populating the bonding state formed from a singly occupied apex dangling bond with charge removed from the scanned atom underneath the tip.

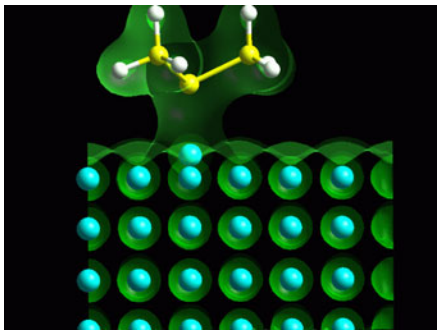

Figure 2. The chemical bond between a Cu(001) surface and a pure Si tip.

This short-range covalent interaction would lead, provided stable imaging is possible (see below), to FM–AFM images with normal contrast: the positions of the atoms correspond to the protrusions. Notice, however, that the delocalized nature of the metal surface wavefunctions is reflected in some features of the total energy and force curves. At variance with semiconducting surfaces, the absolute minimum of the total energy is over the hollow site. This is related to the short distances between nearest neighbour atoms on the metal surface that favour high coordination sites, in spite of the strongly localized character of the tip dangling bond.

One consequence of this localized covalent bonding situation is that, in the on-top position, there is a large surface response with the surface Cu atom so strongly bonded to the tip that it follows the apex (figures 2, 3). This ultimately leads to the creation of a vacancy and modification of the tip–apex. During this process the tip–apex is also deformed (figure 3). Hence, this tip–surface interaction would *not* lead to a stable imaging with the atomic resolution found in the experiments [25, 26]. Similarly the strength of the computed force and its range are both incompatible with the results measured in the experiments [26]. A better insight may be gained from a computer graphics animation [42]. We note that the extraction of a surface atom may be even more likely from other surfaces, e.g. gold. This gives further support to the suggestions made in connection with explanation of the STM images of metals [30].

These results suggest that the experimental images may correspond to metal contaminated tips. Figures 1(b), (c) show the results for two tips where the apex has been modified with the inclusion of a Cu atom. None of the two tips would remove the imaged Cu atom from the surface in line with the reduced amount of induced charge and weaker tip–sample interaction energy. Both apices should provide a rather stable imaging, albeit with hollow sites appearing as protrusions. This inverted contrast is a consequence of the more delocalized

[3] We used a CASTEP 4.2 (academic version) suite of programs; for the theory behind this code see [35–37].

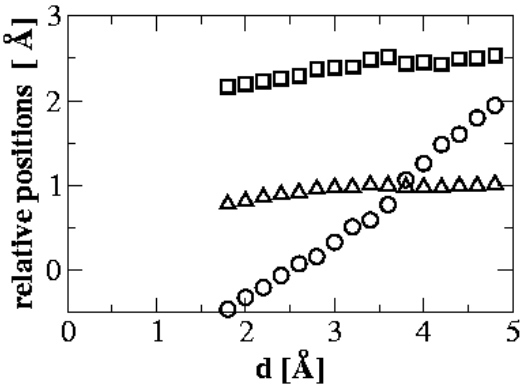

Figure 3. The evolution of relevant distances for a scan with a pure Si tip (figure 1 (a)): removed Cu atom–surface (circles), Si apex-removed Cu atom (squares), and Si apex–tip base (triangles) as a function of tip position.

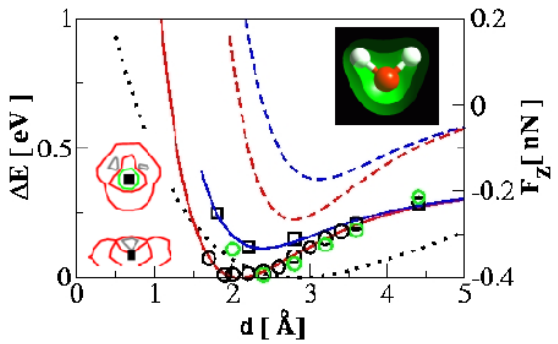

Figure 4. Vertical scans with the model H_2O tip. The labelling of the curves and right inset is as in figure 1; black (green) circles represent lone-pair orbitals parallel (perpendicular) to the surface. The dotted curve shows the experimentally determined chemical force [26] with minimum shifted horizontally to coincide with the position in the computed curves. The left inset shows the induced charge density $(\rho(\mathbf{r})_{\text{tip–sample}}-\rho(\mathbf{r})_{\text{tip}}-\rho(\mathbf{r})_{\text{sample}})$ around the apex/scanned atom (black boxes) due to tip–sample interaction (red, zero; black, charge pile up; green, charge depletion).

character of the Cu wavefunctions as compared to the Si dangling bond. The apex with the Cu atom removed from the surface appears to be more compliant. On approach, the Cu apex deforms and forms inequivalent bonds to two adjacent surface atoms. Despite providing stable imaging, both types of tip–surface interactions correspond to *strong imaging* which cannot account for the experimentally determined chemical interaction.

The discrepancy between the measured weak short-range forces and the strong ones calculated with both the clean and metal contaminated Si tips indicates that a different tip has been used for the imaging. Based on the experimental resistance measurements [26], the existence of a thin oxide layer on the tip can be assumed. Figure 4 shows the results for the simple model, a water molecule, we have considered to describe this tip termination. As explained below, the oxygen lone-pair electrons play a crucial role in this type of tip–surface interaction. For that reason we have considered two model tip orientations, namely perpendicular and parallel to the surface. With this model we find that, while the range of the calculated force is shorter than in the experiment, its strength is in the experimental range, suggesting that an oxidized tip is actually used in the experiments.

4. Discussion and conclusions

The comparison between the measured short-range forces and our theoretical calculations indicate that the imaging of metal surfaces was *not* done using strong covalent tip–surface forces but rather a weak interaction, related to the interaction of a closed-shell electronic density like that of an oxidized Si tip with the metal wavefunctions.

Notice that the description of this kind of bonding is particularly difficult even with simplified models. In spite of strong experimental and theoretical efforts, the interaction of H_2O with metal surfaces is not entirely understood [43]. The weak interaction results from three types of interactions: (1) van der Waals, (2) dipole–dipole, and (3) charge transfer interaction. Of these, the last one is generally the strongest. The strength of this interaction critically depends on the ionization potential of the tip and the electron affinity of the metal. The ionization potential of water is very high, and results from the lone-pair orbital of water. As is shown in figure 4, the result is a charge transfer from the tip to the metal surface. The lone-pair orbital is oriented parallel to the surface when the H_2O model tip is oriented perpendicular to the surface (cf the inset of figure 4). Notice that changing the orientation of the lone-pair orbitals with respect to the surface from parallel to perpendicular moves the minimum of the energy curve by about ∼0.5 Å (cf figure 4). The charge transfer process follows the motion of the tip–apex and is entirely reversible. The net effect of the electric field due to the *reversible charge transfer* between the tip and the surface (figure 4) is *weak*. Given the simplicity of the model, the calculated results give a fair reproduction of the strength of the interaction which are in reasonable agreement with the experiments. From the above discussion of the lone-pair orbital orientation we expect that a more realistic tip termination with more O atoms interacting with the surface would result in a convolution of the curve and further improvement of the agreement with the experiment. A similar effect is also expected from a more realistic treatment of the dispersive interactions.

This new imaging mechanism that we have found for oxidized Si tips is very different from the other mechanisms identified here or on semiconductor surfaces [12]. In those cases an induced charge pile-up occurs between the tip and the surface atom(s) whose amount determines the strength of the tip–surface interaction. The bonding of the model water tip, analysed in figure 5, shows that the tip–surface overlap is extremely weak. Because of the large ionization potential of water the situation is only little altered if a more favourable orientation of the lone-pair orbitals to the surface is considered (cf figure 4). This provides an explanation for the experimentally found, but not fully understood, relation $\lambda_F = 2\lambda_T$ [26] between the force and tunnelling current decay lengths. Such a relation has been proposed by Chen [44] assuming weak electronic tip–surface overlap. Use of this *weak imaging*, where possible, has the advantage over the strong imaging of only negligibly perturbing the sample. We expect this imaging to work equally well on reactive semiconductor surfaces.

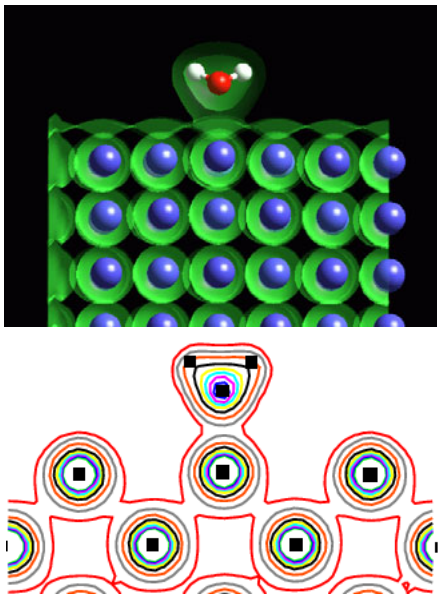

Figure 5. The interaction of the H_2O model tip with the Cu(100) surface. Upper panel: ball and stick model with two superimposed isosurfaces of constant valence electronic charge density; lower panel: contour plot of the total valence electronic charge density.

In conclusion, we have performed the first simulation of the FM–AFM image formation on metallic surfaces. We find that the most natural tip terminations yield very strong covalent tip–surface interaction, indistinguishable from that typically found on semiconductor surfaces. Hence, atomic-scale imaging for both types of materials may result from the same mechanism of a strong covalent tip–surface interaction. A completely different stable imaging was found to result from weak *reversible short-range electrostatic charge-transfer imaging* which, in turn, provides an explanation for the experimentally observed double decay length for AFM, compared to STM. Our work shows that apex engineering, assisted by computer modelling, may help to optimize the imaging mechanism by identifying tip terminations maximizing surface corrugation while simultaneously minimizing the perturbation to the measured surface and formation of unstable tips.

Acknowledgments

The authors gratefully acknowledge fruitful discussions with R Bennewitz and A Baratoff (University of Basel, Switzerland) and Ch Loppacher (University of Technology Dresden, Germany).

References

[1] Giessibl F J 1994 *Japan. J. Appl. Phys.* **33** 3726
[2] Giessibl F J 1995 *Science* **267** 68
[3] Kitamura S and Iwatsuki M 1996 *Japan. J. Appl. Phys.* **35** L668
[4] Sugawara Y *et al* 1995 *Science* **270** 1646
[5] Ueyama H *et al* 1995 *Japan. J. Appl. Phys.* **34** L1086
[6] Ohta M *et al* 1995 *J. Vac. Sci. Technol.* B **13** 1265
[7] Schwarz A *et al* 1999 *Appl. Surf. Sci.* **140** 293
[8] Bammerlin M *et al* 1997 *Probe Microsc.* **1** 3
[9] Jarvis S P *et al* 1996 *Nature* **384** 247
[10] Garcia R and Perez R 2002 *Surf. Sci. Rep.* **47** 197
[11] Giessibl F J 2003 *Rev. Mod. Phys.* **75** 949
[12] Pérez R, Payne M C, Štich I and Terakura K 1997 *Phys. Rev. Lett.* **78** 678
[13] Pérez R, Štich I, Payne M C and Terakura K 1998 *Phys. Rev.* B **58** 10835
[14] Ke S H, Uda T, Pérez R, Štich I and Terakura K 1999 *Phys. Rev.* B **60** 11631
[15] Tóbik J, Štich I, Pérez R and Terakura K 1999 *Phys. Rev.* B **60** 11639
[16] Tóbik J, Štich I and Terakura K 2001 *Phys. Rev.* B **63** 245324
[17] Uchihashi T *et al* 1997 *Phys. Rev.* B **56** 9834
[18] Erlandsson R, Olsson L and Mårtenson P 1996 *Phys. Rev.* B **54** R8309
[19] Lantz M A *et al* 2000 *Phys. Rev. Lett.* **84** 2642
[20] Lantz M A *et al* 2001 *Science* **291** 2580
[21] Eguchi T and Hasegawa Y 2002 *Phys. Rev. Lett.* **89** 266105
[22] Livshits A I *et al* 1999 *Phys. Rev.* B **59** 2436
[23] Foster A S *et al* 2001 *Phys. Rev. Lett.* B **86** 2373
[24] Foster A S *et al* 2002 *Phys. Rev.* B **66** 235417
[25] Loppacher Ch *et al* 1999 *Appl. Surf. Sci.* **140** 287
[26] Loppacher Ch *et al* 2000 *Phys. Rev.* B **62** 16944
[27] Orisaka S *et al* 1999 *Appl. Surf. Sci.* **140** 243
[28] Hallmark V M *et al* 1987 *Phys. Rev. Lett.* **59** 2879
[29] Wintterlin J *et al* 1989 *Phys. Rev. Lett.* **62** 59
[30] Ciraci S *et al* 1992 *Phys. Rev.* B **46** 10411
[31] Dieška P, Štich I and Pérez R 2003 *Phys. Rev. Lett.* **91** 216401
[32] Guggisberg M *et al* 2000 *Phys. Rev.* B **61** 11151
[33] See, for instance, Rignanese G-M *et al* 2000 *Phys. Rev.* B **61** 13250
[34] Ke S-H, Uda T and Terakura K 2002 *Phys. Rev.* B **65** 125417
[35] See, for instance, Payne M C *et al* 1992 *Rev. Mod. Phys.* **64** 1045
[36] Vanderbilt D 1990 *Phys. Rev.* B **41** 7892
[37] Kresse G and Furthmüller J 1996 *Phys. Rev.* B **54** 11169
Bowler D R and Gillan M J 2000 *Chem. Phys. Lett.* **325** 473–6
[38] Perdew J P *et al* 1992 *Phys. Rev.* B **46** 6671
[39] Monkhorst H J and Pack J D 1976 *Phys. Rev.* B **13** 5188
[40] Gillan M J 1989 *J. Phys.: Condens. Matter* **1** 689
[41] Jarvis M R *et al* 1997 *Phys. Rev.* B **56** 14972
[42] A computer graphics animation of the simulation can be downloaded from
http://www.ccms.elf.stuba.sk/ra_afm.html
[43] Henderson M A 2002 *Surf. Sci. Rep.* **46** 1
[44] Chen C J 1992 *Introduction to Scanning Tunneling Microscopy* (New York: Oxford University Press) chapter 7